Applied Physics Letters

Perfect acoustic bandgap metabeam based on a quadruple-mode resonator array

Cite as: Appl. Phys. Lett. **115**, 081905 (2019); https://doi.org/10.1063/1.5117283
Submitted: 02 July 2019 . Accepted: 31 July 2019 . Published Online: 23 August 2019

Kentaro Fujita, Motonobu Tomoda, Oliver B. Wright, and Osamu Matsuda

Applied Physics Letters ARTICLE scitation.org/journal/apl

Perfect acoustic bandgap metabeam based on a quadruple-mode resonator array

Cite as: Appl. Phys. Lett. **115**, 081905 (2019); doi: 10.1063/1.5117283
Submitted: 2 July 2019 · Accepted: 31 July 2019 ·
Published Online: 23 August 2019

Kentaro Fujita, Motonobu Tomoda,[a] Oliver B. Wright, and Osamu Matsuda[b]

AFFILIATIONS

Division of Applied Physics, Graduate School of Engineering, Hokkaido University, Sapporo 060-8628, Japan

[a]Electronic mail: mtomoda@eng.hokudai.ac.jp
[b]Electronic mail: omatsuda@eng.hokudai.ac.jp

ABSTRACT

Solid structures guide a multitude of elastic modes of different polarizations including both compression and shear, and the nature of the elastic constant tensor implies a much richer behavior than in optics. Here, we introduce a metamaterial in the form of a rectangular cross section beam of a single isotropic material that can simultaneously suppress all elastic-wave polarizations in the beam over a range of frequencies in the kHz range. This is experimentally achieved by machining replicas of a subwavelength unit cell in an aluminum metabeam based on a planar resonator with interconnected ribs, showing complex vibrational degrees of freedom that allow it to couple to compressional, in-plane shear, flexural and torsional vibrations, that is, all four existing mode types. The result is a lightweight structure that can forbid all possible acoustic modes over the metamaterial bandgap frequency range, an exotic behavior that opens up diverse applications in easily manufacturable vibration isolation structures and acoustic wave control.

Electromagnetic metamaterials consisting of subwavelength resonators that show effective negative permeability and permittivity have led to a wealth of applications since they were first proposed 20 years ago.[1–3] Around the same time, acoustic metamaterials showing effective negative density and modulus were introduced.[4] In the acoustic case, many studies have focused on various nonintuitive phenomena such as negative refraction,[5,6] superlensing,[7–9] and cloaking.[10–13] But applications in sound damping appear to be the most promising for practical applications.[14–32] In spite of this progress, the development of useful damping materials in the form of metamaterial beams or rods, i.e., metabeams or metarods, which simultaneously block different acoustic polarizations, has not proved to be an easy task.[17–32] The problem stems from acoustic waveguide structures possessing multiple acoustic modes. A case in point are rectangular beams, which exhibit four modes, i.e., compressional, shear-horizontal (i.e., in-plane shear), shear-vertical (i.e., flexural), and torsional modes.[33–35]

Many studies of metabeam or rod damping involve only flexural modes. For example, Yu *et al.* proposed a geometry of annular resonators fixed at regular intervals on a metallic rod, Xiao *et al.* proposed a geometry of metallic rectangular beams with attached metallic resonator plates,[17,19] and Nouh *et al.* and Zhang *et al.* proposed beams with periodically spaced membrane resonator inclusions.[22,23] Other designs that attenuate flexural modes were proposed by Zhu *et al.*, who made use of a thin metallic ligament chiral lattice with added masses,[21] and by Tang and Cheng, who made use of square beams of steel with lens-shaped hole arrays.[28]

Damping of other modes in metamaterial beams and rods has also been investigated. Nobrega *et al.* proposed rectangular plastic beams with embedded metal mass resonators to attenuate compressional modes.[27] To damp torsional modes, Li and Cai proposed circular epoxy rods surrounded by rubber springs and epoxy ring masses,[26] and Wang *et al.* proposed epoxy rods surrounded by periodic resonators.[32]

However, for practical applications, it is advantageous to block all acoustic polarizations. Numerical simulations for square cross section rods that block three acoustic polarizations, yielding a perfect bandgap in a given finite frequency range, were reported by Ma *et al.* who used epoxy rods containing silicone-coated steel masses;[24] however, the existence of a perfect bandgap for all modes was not demonstrated experimentally.

Another line of approach in this field has been to simplify fabrication by choosing a single material for metabeams or metarods. Out of the above quoted studies, only that of Tang and Cheng has involved a single material.[28] In spite of the example set by perfect-bandgap phononic crystal beams or rods, which possess periodicities comparable to the acoustic wavelength,[36–41] no single-material metamaterial beams or rods that can block all acoustic polarizations have been proposed.

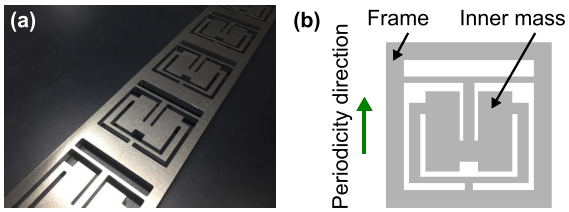

FIG. 1. Metabeam design. (a) Photograph of the metamaterial beam. (b) Schematic of the top view of the unit cell. The gray region is aluminum, and the inner white areas are holes. The unit-cell geometry comprises a frame, an inner mass, and several ribs.

TABLE I. Symmetry (S: symmetric and A: antisymmetric) of the deformations associated with acoustic modes in rectangular cross section beams.

Mode	Along the width	Over the depth
Compressional	S	S
Shear-horizontal	A	S
Shear-vertical	S	A
Torsional	A	A

Here, we not only experimentally demonstrate a perfect-bandgap acoustic metabeam but also show that this can be achieved with a single material. Inspired by mass-spring resonator metamaterials, we make use of a complex unit cell in a rectangular-cross section beam consisting of interconnected ribs and a central mass. Guided by approximate analytical models, we tailor compressional, in-plane shear, flexural, and torsional resonances to form a single perfect bandgap that allows all these polarizations to be blocked. The chosen design, made of aluminum, is first verified by numerical simulation and then by measurements on all four modes at frequencies in the kHz range.

A photograph of the proposed metabeam is shown in Fig. 1(a). The structure consists of an aluminum (dural A2017) plate of thickness 8.0 mm and width 80.0 mm with a periodic drilled pattern of square unit cells at a repeat distance of 80.0 mm. The drilled sections are perpendicular to the top and bottom surfaces of the beam. Figure 1(b) shows a schematic diagram of a single unit cell (see the supplementary material for a detailed description). It consists of an outer frame and an inner geometry with a resonating inner mass supported by several perpendicular interconnected ribs that function as springs. As previously mentioned, isotropic rectangular beams possess four acoustic modes of different polarization propagating along the axial direction, which can be classified by the symmetry of the acoustic deformations along the width and over the depth in the beam, as shown in Table I. Our strategy is to set the lowest resonance for each of the four polarizations to roughly the same frequency in order to open a perfect bandgap. The roles of the ribs and configuration of the inner mass in the proposed geometry are different for each polarization, as described below. We first present numerical simulations of the optimized design and then experimental results for acoustic attenuation in a 10-unit-cell beam. Simulations of the acoustic attenuation are then presented.

The approximate roles of the springs for each of the four polarizations are shown in Figs. 2(a)–2(d), which can be better understood with reference to the on-resonance results of finite-element numerical simulations with COMSOL Multiphysics (version 5.4) for a single unit cell with two fixed boundaries perpendicular to the axial direction: we show kinetic- and strain-energy density plots in Figs. 2(f)–2(m) (animation also viewable in the supplementary material). The

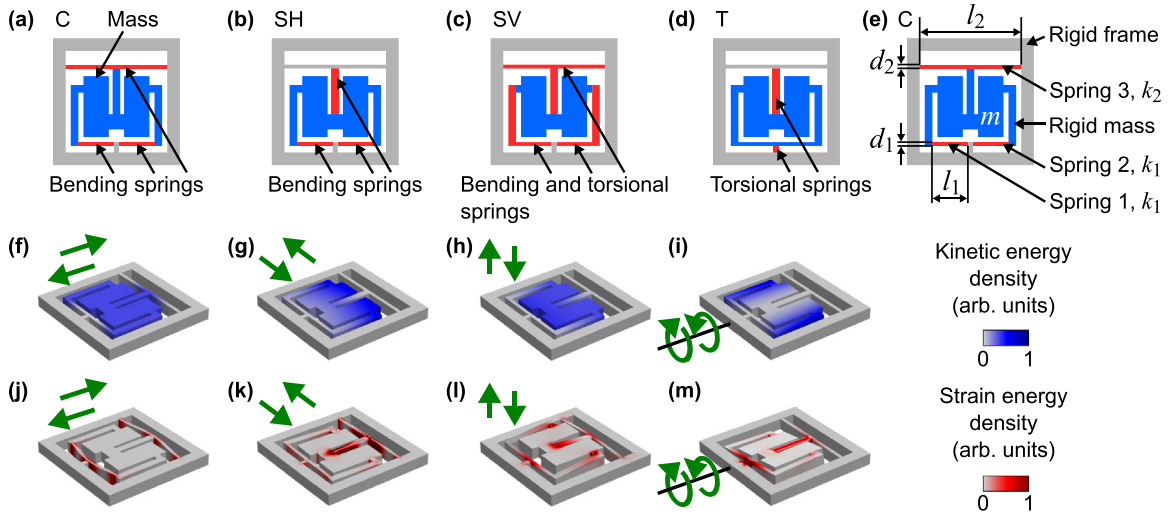

FIG. 2. Approximate analytical interpretation of the beam geometry in terms of masses and springs and simulated single-cell acoustic eigenmodes with rigid boundary conditions. (a)–(d) Geometries used for the models. The blue regions and red ribs act as masses and springs, respectively, shown for the following modes: (a) compressional (C, motion along the axial direction), (b) shear-horizontal (SH, motion along the width direction), (c) shear-vertical (SV, out-of-plane flexural motion), and (d) torsional (T, rotation about the axis along the axial direction). The gray regions are assumed to be rigid in the analytical models. (e) Detailed geometry for the compressional mode, showing the rigid inner mass m and springs 1, 2, and 3. The gray region is considered to be a rigid frame. Only in-plane motion along the axial direction is considered. (f)–(i) and (j)–(m): simulated kinetic- and strain-energy distributions for the lowest four eigenmodes, respectively. The green arrows show the displacements.

corresponding resonance frequencies, 0.91, 0.99, 1.01, and 0.98 kHz, are all tuned close to 1 kHz by iterative simulation of the rib and inner mass dimensions. The density, longitudinal sound velocity, and transverse sound velocity of the beam are taken to be 2.79×10^3 kg m^{-3}, 6.32×10^3 m s^{-1}, and 3.13×10^3 m s^{-1},[42] respectively, and internal friction is ignored. As shown by the green arrows, for the compressional resonance the inner mass vibrates along the axial direction, for the shear-horizontal resonance it swings along the width direction, for the shear-vertical resonance it vibrates along the depth direction, and for the torsional resonance it rotates about the central axis of the beam. In this way, a quadruple-mode resonant structure is created.

It is pertinent to investigate the dependence of each of the resonant frequencies on the chosen geometrical parameters by means of approximate analytical or semianalytical models. Consider the case of the compressional resonance, as illustrated schematically in Fig. 2(e) (see the supplementary material for the other modes). The (blue) inner mass m is assumed to be connected to an outer (gray) rigid frame by (red) bending springs, two of them (1, 2) of spring constant k_1 and one of them (3) of spring constant k_2, with the former two springs being identical. Assuming low-amplitude bending, the spring constants can be written as $k_1 = (Ed_1^3 t)/l_1^3$ and $k_2 = (16Ed_2^3 t)/l_2^3$, where E is Young's modulus, t is the beam thickness, and l_i and d_i are the length and width of springs 1 and 2 ($i = 1$) and 3 ($i = 2$), respectively. Since the three springs act in parallel, the resonant frequency is given by $f = (1/2\pi)[(2k_1 + k_2)/m]^{1/2}$, where $l_1 = 22.4$ mm, $l_2 = 64.0$ mm, $d_1 = d_2 = 2.4$ mm, $t = 8.0$ mm, $m = 4.15 \times 10^{-2}$ kg, and $E = 73.1$ GPa. The value $f = 1.09$ kHz obtained is in fair agreement with $f = 0.91$ kHz from simulation, considering the approximations made. Reasonable agreement between the analytical models and numerical simulations is also obtained for the other three vibrational modes, confirming the mass-spring interpretation of the dynamics (see the supplementary material).

The numerically derived dispersion relation using periodic boundary conditions is shown in Fig. 3, showing the existence of a perfect bandgap from 0.97 kHz to 1.09 kHz arising from local resonances, where the bandgaps for the four modes overlap. Strikingly, in spite of the beam being able to guide four different acoustic polarizations, this structure damps out *all* of these axially propagating acoustic disturbances in the bandgap region. The onset of each bandgap occurs at a frequency similar to the resonant frequency for the corresponding mode derived above for a single unit cell.

We measure the acoustic propagation characteristics for all four modes by means of a 10-unit-cell metabeam that is 80.0 cm in length. The experiment for the compressional mode is described here and those for the other three modes in the supplementary material. The apparatus is shown in Fig. 4. The sample, vertically suspended by fishing line, is excited by a sinusoidally driven piezoelectric disk (Murata Manufacturing 7BB-41-2L0) bonded on one end. Three-axis accelerometers (Fuji Ceramics SA12ZSCA) are used at two points at both ends of the metabeam [see red squares in Fig. 4(a)] in conjunction with lock-in detection, in order to obtain a measure of the acoustic wave damping.

The experimental output/input amplitude ratio for all four modes is shown on a logarithmic scale in Fig. 5. Outside the bandgap in each case, interference by multiple acoustic reflections occurs, producing local maxima and minima, but all modes show marked damping in the bandgap regions. It is difficult to precisely determine the perfect

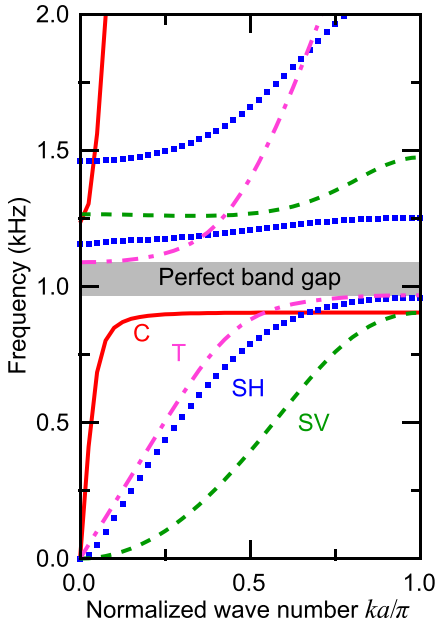

FIG. 3. Acoustic dispersion relation for axial propagation in the metabeam; k and a are the wavevector and unit-cell length, respectively. The solid red, dotted blue, dashed green, and dashed-dotted pink curves correspond to compressional (C), shear-horizontal (SH), shear-vertical (SV), and torsional (T) modes, respectively.

bandgap experimentally, but the output/input ratio takes a value less than 0.5 between 1.02 and 1.16 kHz, which is in reasonable correspondence with the simulated perfect-bandgap region.

Numerical simulations can be used to compare with the observed damping. We assume there is a vacuum outside the sample in the simulations. Simulated effective amplitude decay constants derived from the output/input amplitude ratio for a free-standing 10-unit-cell metabeam are shown in Figs. 6(a)–6(d) together with those derived from experiment (see the supplementary material for the details of the simulations). The order of magnitude of the simulated decay constants is in reasonable agreement with those from experiment. We attribute the differences to small imperfections in fabrication, to residual sound

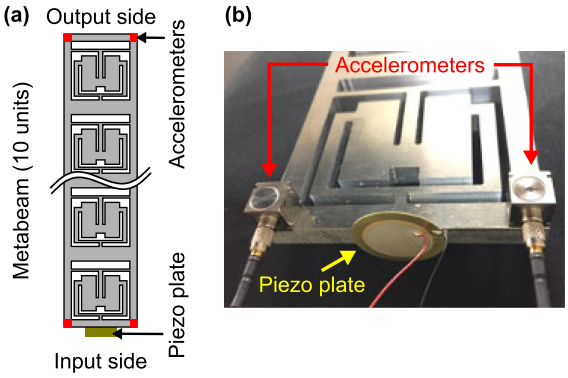

FIG. 4. Experimental setup. (a) Schematic diagram of the setup for compressional mode propagation measurements. (b) Image showing the compressional mode excitation.

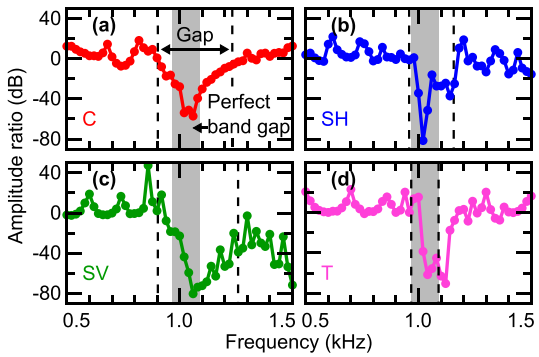

FIG. 5. Experimentally observed output/input acoustic amplitude ratio for each acoustic mode. (a)–(d) correspond to the compressional, shear-horizontal, shear-vertical (flexural), and torsional modes, respectively. The vertical dashed lines indicate the band edges for each mode expected from the simulations, whereas the gray shaded region in each case corresponds to the perfect bandgap expected from the simulations.

transmitted through the air or to perturbations caused by the added masses of the accelerometers. As previously mentioned, data outside the gap regions are heavily influenced in both experiment and simulation by multiple acoustic reflections along the beam and are not reliable for quantitative analysis, but the correspondence between experiment and simulation in these regions is also reasonable. The particularly pronounced peak for the simulation evident for the compressional mode in Fig. 6(a) near the band onset arises because only this mode exhibits a marked near-zero group velocity branch just above the band onset. At ∼1 kHz, the typical experimental decay constant, ∼5 m^{-1} for all modes, implies that acoustic attenuation across 10 unit cells is sufficient to almost completely damp out the acoustic amplitude by a factor of ∼50.

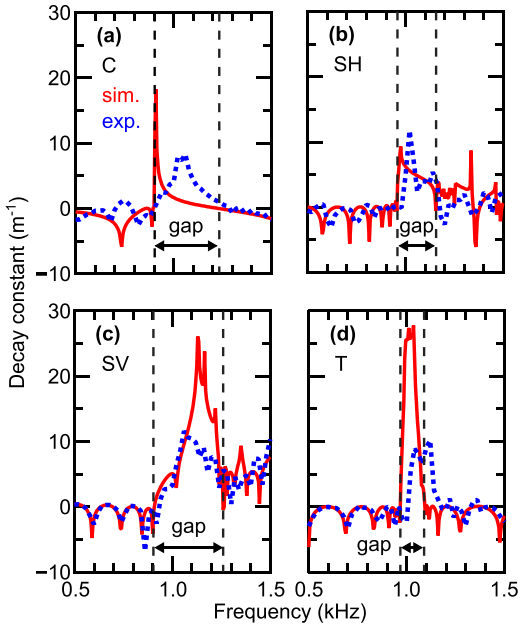

FIG. 6. Results of simulations and experiments for a metabeam of 10 unit cells. Comparison of the experimentally obtained decay constants (dotted blue lines) with those obtained from simulation (solid red lines) for the four modes. (a)–(d) show the results for the compressional (C) mode, shear horizontal (SH) mode, shear vertical (SV) mode, and torsional (T) mode, respectively. The vertical dashed lines indicate the band edges obtained from the simulated dispersion relations. sim.: simulation; exp.: experiment.

The observed properties of the metabeam originate solely from its metamaterial nature, i.e., they depend on local resonances rather than on periodicity; varying the lattice constant through the thickness of the portions of the frames separating unit cells merely affects the bandgap widths while not significantly changing the bandgap central frequencies (see the supplementary material, where the effect of changing the frame thickness is analyzed).

In conclusion, we have demonstrated both experimentally and by simulation a lightweight single-material metabeam made of aluminum with a rectangular cross section in the form of a periodic quadruple-mode resonator array that displays a perfect acoustic bandgap near 1 kHz. In this region, our structure efficiently damps out compressional, in-plane shear, flexural and torsional vibrations, as predicted by the simulations.

The frequency range for acoustic damping demonstrated here should be extendable to wider band operation by the use of a gradient in unit cell properties along the length of the metabeam. In addition, lower frequencies may be accessed without a proportional increase in the weight by the use of softer materials such as rubber, which could provide effective damping of low frequency vibrations in machinery or vehicles, for example. Further, truly large scale extension of the present type of geometry may well prove to be useful in earthquake vibration isolation for buildings and structures.

See the supplementary material for the detailed structure, approximate analytical models, experimental setup, simulations, and decay constants as well as the animation for the motion of each mode.

We acknowledge Grants-in-Aid for Scientific Research from the Japan Society for the Promotion of Science and a research grant from Insight K.K., Japan. We are also grateful to Yuji Mori in the Technical Center, Faculty of Engineering, Hokkaido University for the fabrication of the metabeam, and to Eun Bok and Sam Hyeon Lee of Yonsei University for valuable discussions on metamaterials.

REFERENCES

[1]J. B. Pendry, A. J. Holden, D. J. Robbins, W. Stewart *et al.*, "Magnetism from conductors and enhanced nonlinear phenomena," IEEE Trans. Microwave Theory Tech. **47**, 2075–2084 (1999).
[2]D. R. Smith, W. J. Padilla, D. Vier, S. C. Nemat-Nasser, and S. Schultz, "Composite medium with simultaneously negative permeability and permittivity," Phys. Rev. Lett. **84**, 4184 (2000).
[3]R. A. Shelby, D. R. Smith, and S. Schultz, "Experimental verification of a negative index of refraction," Science **292**, 77–79 (2001).
[4]Z. Liu, X. Zhang, Y. Mao, Y. Zhu, Z. Yang, C. T. Chan, and P. Sheng, "Locally resonant sonic materials," Science **289**, 1734–1736 (2000).
[5]V. M. García-Chocano, J. Christensen, and J. Sánchez-Dehesa, "Negative refraction and energy funneling by hyperbolic materials: An experimental demonstration in acoustics," Phys. Rev. Lett. **112**, 144301 (2014).
[6]R. Zhu, X. Liu, G. Hu, C. Sun, and G. Huang, "Negative refraction of elastic waves at the deep-subwavelength scale in a single-phase metamaterial," Nat. Commun. **5**, 5510 (2014).

[7]S. Zhang, L. Yin, and N. Fang, "Focusing ultrasound with an acoustic metamaterial network," Phys. Rev. Lett. **102**, 194301 (2009).
[8]L. Zigoneanu, B.-I. Popa, and S. A. Cummer, "Design and measurements of a broadband two-dimensional acoustic lens," Phys. Rev. B **84**, 024305 (2011).
[9]F. Lemoult, N. Kaina, M. Fink, and G. Lerosey, "Soda cans metamaterial: a subwavelength-scaled phononic crystal," Crystals **6**, 82 (2016).
[10]J. Pendry and J. Li, "An acoustic metafluid: realizing a broadband acoustic cloak," New J. Phys. **10**, 115032 (2008).
[11]A. N. Norris, "Acoustic metafluids," J. Acoust. Soc. Am. **125**, 839–849 (2009).
[12]N. Stenger, M. Wilhelm, and M. Wegener, "Experiments on elastic cloaking in thin plates," Phys. Rev. Lett. **108**, 014301 (2012).
[13]T. Bückmann, M. Thiel, M. Kadic, R. Schittny, and M. Wegener, "An elasto-mechanical unfeelability cloak made of pentamode metamaterials," Nat. Commun. **5**, 4130 (2014).
[14]N. Fang, D. Xi, J. Xu, M. Ambati, W. Srituravanich, C. Sun, and X. Zhang, "Ultrasonic metamaterials with negative modulus," Nat. Mater. **5**, 452 (2006).
[15]S. Yao, X. Zhou, and G. Hu, "Experimental study on negative effective mass in a 1d mass–spring system," New J. Phys. **10**, 043020 (2008).
[16]P. H. Otsuka, S. Mezil, O. Matsuda, M. Tomoda, A. A. Maznev, T. Gan, N. Fang, N. Boechler, V. E. Gusev, and O. B. Wright, "Time-domain imaging of gigahertz surface waves on an acoustic metamaterial," New J. Phys. **20**, 013026 (2018).
[17]D. Yu, Y. Liu, G. Wang, H. Zhao, and J. Qiu, "Flexural vibration band gaps in timoshenko beams with locally resonant structures," J. Appl. Phys. **100**, 124901 (2006).
[18]Y. Xiao, J. Wen, D. Yu, and X. Wen, "Flexural wave propagation in beams with periodically attached vibration absorbers: band-gap behavior and band formation mechanisms," J. Sound Vib. **332**, 867–893 (2013).
[19]Y. Xiao, J. Wen, G. Wang, and X. Wen, "Theoretical and experimental study of locally resonant and bragg band gaps in flexural beams carrying periodic arrays of beam-like resonators," J. Vib. Acoust. **135**, 041006 (2013).
[20]S. Zhang, J. Hui Wu, and Z. Hu, "Low-frequency locally resonant band-gaps in phononic crystal plates with periodic spiral resonators," J. Appl. Phys. **113**, 163511 (2013).
[21]R. Zhu, X. Liu, G. Hu, C. Sun, and G. Huang, "A chiral elastic metamaterial beam for broadband vibration suppression," J. Sound Vib. **333**, 2759–2773 (2014).
[22]M. Nouh, O. Aldraihem, and A. Baz, "Vibration characteristics of metamaterial beams with periodic local resonances," J. Vib. Acoust. **136**, 061012 (2014).
[23]H. Zhang, Y. Xiao, J. Wen, D. Yu, and X. Wen, "Flexural wave band gaps in metamaterial beams with membrane-type resonators: theory and experiment," J. Phys. D: Appl. Phys. **48**, 435305 (2015).
[24]G. Ma, C. Fu, G. Wang, P. Del Hougne, J. Christensen, Y. Lai, and P. Sheng, "Polarization bandgaps and fluid-like elasticity in fully solid elastic metamaterials," Nat Commun. **7**, 13536 (2016).
[25]T. Wang, M.-P. Sheng, and Q.-H. Qin, "Multi-flexural band gaps in an Euler–Bernoulli beam with lateral local resonators," Phys. Lett. A **380**, 525–529 (2016).
[26]L. Li and A. Cai, "Low-frequency band gap mechanism of torsional vibration of lightweight elastic metamaterial shafts," Eur. Phys. J. Appl. Phys. **75**, 10501 (2016).
[27]E. Nobrega, F. Gautier, A. Pelat, and J. Dos Santos, "Vibration band gaps for elastic metamaterial rods using wave finite element method," Mech. Syst. Signal Process. **79**, 192–202 (2016).
[28]L. Tang and L. Cheng, "Ultrawide band gaps in beams with double-leaf acoustic black hole indentations," J. Acoust. Soc. Am. **142**, 2802–2807 (2017).
[29]H. Chen, X. Li, Y. Chen, and G. Huang, "Wave propagation and absorption of sandwich beams containing interior dissipative multi-resonators," Ultrasonics **76**, 99–108 (2017).
[30]J.-S. Chen, Y.-J. Huang, and I.-T. Chien, "Flexural wave propagation in metamaterial beams containing membrane-mass structures," Int. J. Mech. Sci. **131–132**, 500–506 (2017).
[31]L. Li, R. Lv, A. Cai, M. Xie, Y. Chen, and G. Huang, "Low-frequency vibration suppression of a multi-layered elastic metamaterial shaft with discretized scatters," J. Phys. D: Appl. Phys. **52**, 055105 (2019).
[32]K. Wang, J. Zhou, D. Xu, and H. Ouyang, "Tunable low-frequency torsional-wave band gaps in a meta-shaft," J. Phys. D: Appl. Phys **52**, 055104 (2019).
[33]N. J. Nigro, "Steady-state wave propagation in infinite bars of noncircular cross section," J. Acoust. Soc. Am. **40**, 1501–1508 (1966).
[34]W. Fraser, "Stress wave propagation in rectangular bars," Int. J. Solids Struct. **5**, 379–397 (1969).
[35]R. D. Mindlin, "Low frequency vibrations of elastic bars," Int. J. Solids Struct. **12**, 27–49 (1976).
[36]F.-C. Hsu, C.-I. Lee, J.-C. Hsu, T.-C. Huang, C.-H. Wang, and P. Chang, "Acoustic band gaps in phononic crystal strip waveguides," Appl. Phys. Lett. **96**, 051902 (2010).
[37]Y. Pennec, B. D. Rouhani, C. Li, J. Escalante, A. Martínez, S. Benchabane, V. Laude, and N. Papanikolaou, "Band gaps and cavity modes in dual phononic and photonic strip waveguides," AIP Adv. **1**, 041901 (2011).
[38]F.-C. Hsu, J.-C. Hsu, T.-C. Huang, C.-H. Wang, and P. Chang, "Reducing support loss in micromechanical ring resonators using phononic band-gap structures," J. Phys. D: Appl. Phys. **44**, 375101 (2011).
[39]D. Feng, D. Xu, G. Wu, B. Xiong, and Y. Wang, "Extending of band gaps in silicon based one-dimensional phononic crystal strips," Appl. Phys. Lett. **103**, 151906 (2013).
[40]D. Feng, D. Xu, G. Wu, B. Xiong, and Y. Wang, "Phononic crystal strip based anchors for reducing anchor loss of micromechanical resonators," J. Appl. Phys. **115**, 024503 (2014).
[41]S. Jiang, H. Hu, and V. Laude, "Low-frequency band gap in cross-like holey phononic crystal strip," J. Phys. D: Appl. Phys. **51**, 045601 (2018).
[42]*CRC Handbook of Chemistry and Physics*, 85th ed., edited by D. R. Lide (CRC Press, 2004).